

# Deformation of Ultra-Thin Diamond-Like Carbon Coatings Under Combined Loading on a Magnetic Recording Head

Michael R. Price · Andrey Ovcharenko ·  
Raj Thangaraj · Bart Raeymaekers

Received: 12 September 2014 / Accepted: 10 October 2014 / Published online: 10 January 2015  
© Springer Science+Business Media New York 2014

**Abstract** Ultra-thin diamond-like carbon (DLC) coatings are used in precision engineering applications, such as magnetic storage devices, to protect intricate structures from wear and corrosion. A DLC coating typically consists of hard amorphous carbon in combination with an inter-layer such as silicon (Si), to improve adhesion to the substrate material. Deformation and delamination of these coatings, even in part, could expose the substrate material and compromise its integrity and functionality. We have implemented a molecular dynamics model to quantify the strength of the interface between an ultra-thin tetrahedral amorphous carbon coating, a Si layer, and a permalloy (NiFe) substrate, under combined normal and tangential loading that mimics accidental contact between the recording head and the disk of a hard drive. We have evaluated the effect of the thickness of the different coating layers on deformation and interfacial strength of the coating during combined loading. The results indicate that deformation occurs primarily in the Si layer, and at the interface between the Ni–Si and the Si–C layers. Permanent separation of the Si and ta-C layers is observed, which gradually increases with multiple combined loading cycles. We find that increasing the Si and carbon layer thickness strengthens the DLC coating. However, increasing the carbon layer thickness has a larger effect on coating strength than increasing the Si layer thickness.

**Keywords** Diamond-like carbon · Recording head · Magnetic storage · Ultra-thin films · Interfacial strength

## 1 Introduction

One of the primary drivers of the magnetic storage industry is the desire for increased storage density [1]. To accommodate this, the magnetic spacing between the read/write element of the recording head and the magnetic layer of the disk must be decreased [2]. Figure 1 shows a schematic of the head–disk interface (HDI). The intricate read/write structures of the recording head and the delicate magnetic layer of the disk are protected from accidental contact during hard drive operation by a tetrahedral amorphous carbon (ta-C) and an amorphous carbon (a-C) coating, respectively. The terms ta-C, a-C, and diamond-like carbon (DLC) are sometimes used interchangeably in the literature [3]. Following Casiraghi et al. [3] and Robertson [4], we define ta-C and a-C to be an amorphous form of carbon with 40–90 % and <40 %  $sp^3$  content, respectively, with both ta-C and a-C considered to be a type of DLC. In recent years, the decrease in the flying height between the recording head and the magnetic disk has turned attention to these protective DLC coatings [5]. Removal of the ta-C coating of the recording head, even in part, may expose the read/write element to corrosion and compromise its function and reliability. A silicon (Si) or silicon nitride (SiN) layer may be used to improve adhesion between the hard ta-C layer and the recording head substrate material [6]. Experimental data show that wear and delamination of the DLC coating occur first at the pole tip area of the recording head, and specifically at the permalloy (NiFe) write shield [7, 8]. The pole tip area consists of the read/write elements and shields and is the portion of the head closest to the disk

M. R. Price · B. Raeymaekers (✉)  
Department of Mechanical Engineering, University of Utah,  
Salt Lake City, UT 84112, USA  
e-mail: bart.raeymaekers@utah.edu

A. Ovcharenko · R. Thangaraj  
Western Digital Corporation, San Jose, CA 95138, USA

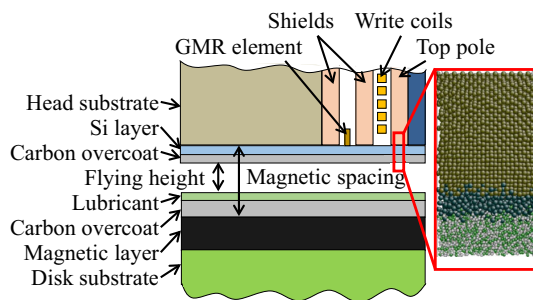


**Fig. 1** Schematic of the head–disk interface, showing the different material layers and structures of the recording head and magnetic disk. The molecular dynamics model, shown as a magnified view, simulates the portion of the recording head indicated by the *box*

during reading and writing. As the thickness of the Si and ta-C layers is reduced to further decrease the magnetic spacing, wear and delamination of these coatings become of increased concern. Thus, an understanding of the deformation and interfacial strength of the protective coating layers of the recording head as a function of operating conditions and coating design parameters is needed. We use a molecular dynamics (MD) approach to simulate the interaction between the different coating layers of a small portion of the HDI indicated by the rectangle in Fig. 1.

Several published studies document and review the mechanical properties of DLC coatings [4, 9–14], with some publications primarily focusing on DLC coatings for hard disk drive (HDD) applications [12–14]. Other works have studied specific aspects of the mechanical properties of the DLC coatings in HDDs. For instance, Prabhakaran and Talke [15] quantified wear of DLC coatings on magnetic recording heads by measuring the change in depth of ion-milled trenches on the surface of the head. They found good correlation of their results with scratch test results. Lee et al. [16] used a capacitive precision actuator to perform nanoindentation of sub-10-nm-thick DLC films deposited on a glass substrate. They measured the hardness of the DLC coating as a function of indentation depth and found an average hardness of 10–15 GPa when the indentation depth remained far enough from the glass substrate. Zhong et al. [17] investigated the mechanical properties and oxidation and corrosion resistance of ultra-thin a-C coatings. They determined a critical minimum coating thickness of 1.4 nm to ensure wear resistance under normal HDD operation, because a coating thinner than 1.4 nm did not significantly reduce the depth of the wear scars compared to those on an uncoated surface. Yasui et al. [18] also characterized sub-2-nm-thick protective DLC coatings on the recording head. They found that the critical normal load for wear resistance during a scratch test depends on the substrate material and the thickness of the

DLC coating but not on the deposition technique of the coating.

As the thickness of the ultra-thin protective DLC coatings is reduced further to accommodate decreasing the magnetic spacing between the recording head and the magnetic disk, experimental characterization becomes increasingly difficult. Consequently, several authors have resorted to stochastic simulation tools, such as MD, to study the mechanical behavior and properties of ultra-thin DLC coatings [19–21]. Evaluating the tribological properties of a-C, ta-C, and thin diamond films has been the objective of several other MD studies. Ma et al. [22] investigated sliding of a-C coatings against a diamond counterface. They found that the low friction coefficient of the interface between a-C and diamond resulted from shear-induced graphitization of the a-C surface, migration of graphitized carbon layers across the sliding interface, and relative motion between the graphitized layers. Gao et al. [23] evaluated the tribological properties of a-C surfaces sliding against a diamond counterface as a function of the properties of the a-C layer. They found that the tribological behavior is highly dependent on the  $sp^3/sp^2$  ratio of the a-C film. Wang and Komvopoulos [24] confirmed this observation. Additionally, Glosli et al. [25] emphasized, based on the MD results, that for ultra-thin coatings <5 nm thick, the mechanical properties are dominated by interfacial phenomena. The primary focus of these MD studies [22–25] is the interaction between the amorphous carbon layer and a rigid diamond counterface.

Although minimizing wear and delamination is of critical importance when decreasing the thickness of DLC coatings on magnetic recording heads, no publications seem to exist that use MD to model and quantify the deformation and interfacial strength of the different layers of the DLC coating of a recording head. Several authors have studied deformation of ultra-thin coatings and delamination from the substrate [26, 27]. However, these studies do not model the materials, interfaces, or operating conditions that occur in a HDD. Thus, the objective of this paper is to evaluate the interfacial strength between the ta-C coating, Si layer, and permalloy substrate as a function of thickness of the different coating layers and the contact pressure during combined normal and tangential loading of the recording head against the magnetic disk. We implement an MD model of a small three-dimensional portion of the HDI, simulating sliding contact between the DLC coating of the recording head and the disk, and we study the interfacial strength of the different coating layers under combined normal and tangential loading. While tailored to the HDI, this study also attempts to provide a general approach and framework for quantifying the strength of the interface between ultra-thin DLC coatings and a substrate.

## 2 Methods

### 2.1 Model

Figure 2 shows the MD model, which consists of a small three-dimensional section of a magnetic recording head, as indicated in Fig. 1, sliding against a hydrogen-terminated diamond counterface. The rigid hydrogen-terminated diamond counterface is used in place of a magnetic disk to reduce the computational cost of the MD simulations and because we focus on deformation of the recording head. However, the shear stress between the head and disk surfaces is similar to that between the recording head and the hydrogenated diamond. The lubricant layer on the disk is not included in our model, and, thus, we simulate a worst-case scenario of contact with lubricant depletion. The recording head substrate consists of a 47 Å Ni layer. While Ni has different magnetic properties than NiFe, its mechanical properties including hardness, Young's modulus, and Poisson ratio are similar [28–31]. Hence, the amount of deformation induced in the substrate, and consequently in the ta-C and Si layers, is not significantly affected by using Ni instead of NiFe. The Ni substrate is covered with a Si layer of thickness  $3 \leq t_{\text{Si}} \leq 9$  Å and a ta-C layer of thickness  $9 \leq t_{\text{C}} \leq 18$  Å. The thickness of the Si and ta-C layers is varied in this study by removing atoms from the middle of the respective layers, thereby ensuring that the ta-C surface, and the interface between ta-C and Si, and Ni and Si are consistent for coatings of different thickness. The  $sp^3$  content of the ta-C coating is 65 % and is constant throughout this study. The ta-C

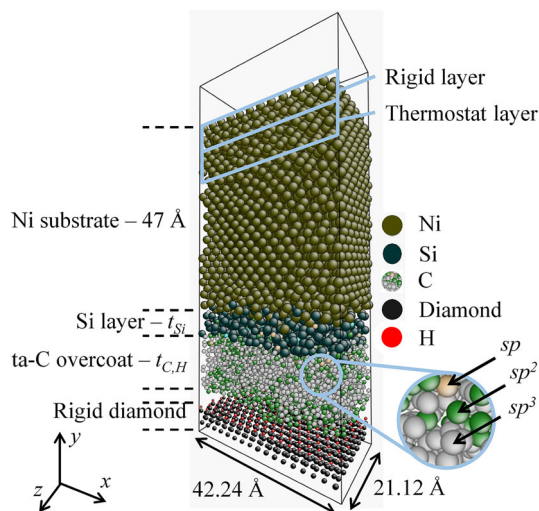


**Fig. 2** Molecular dynamics model of a small portion of the head-disk interface, showing the different material layers of the recording head and the hydrogen-terminated diamond counterface, and their respective thickness. The magnified *inset* shows the different carbon hybridizations in the ta-C layer

coating is formed using a heating and quenching procedure [23, 24]. This process ensures a uniform  $sp^3$  content throughout the ta-C coating. The a-Si layer is created using a similar technique. The simulation box measures  $42.24 \times 100.00 \times 21.12$  Å in  $x$ -,  $y$ -, and  $z$ -directions, respectively, and the model contains between 8,075 and 9,896 atoms, depending on the thickness of the different coating layers. The boundary conditions of the MD model are periodic in the  $x$ - and  $z$ -directions. The three outermost Ni atom layers in the  $y$ -direction are held rigid, and the three adjacent atom layers are maintained at 300 K using a Langevin thermostat to mimic the presence of surrounding bulk material. The hydrogen-terminated diamond counterface is held rigid throughout the simulation. The remaining atoms are free to move according to the micro-canonical ensemble. The interatomic interactions are implemented with the following potentials: MEAM [27, 32] for Ni–Ni and Ni–Si interactions; Tersoff [33] for Si–Si, Si–C, and C–C interactions; and AIREBO [34] for C–H and H–H interactions. The potentials at the interface of coating layers, such as between Tersoff and AIREBO for the C–C and C–H interactions, overlap. The pair coefficients are modified such that when two potentials contribute to the pairwise energy between a single pair type, such as C–C interactions, only one interatomic potential contributes a nonzero energy value. This allows the energy to be calculated correctly even when second-nearest neighbors are modeled using a different potential than first-nearest neighbors. Due to complete separation of the Ni and ta-C layers by the Si layer, there are no first-nearest neighbor Ni–C interactions even in the case of the thinnest silicon layer. However, second-nearest neighbor interactions have been included in the model. We have used the Sandia LAMMPS code to perform the MD simulations [35]. A time step of 0.25 fs is used, and equilibration at 300 K for 10 ps is performed for all simulations.

### 2.2 Simulation Procedure

Figure 3 shows combined normal and tangential loading of the recording head on the disk, which simulates accidental contact. The diamond counterface moves relative to the recording head, at a constant speed of 75 m/s in the  $x$ -direction (step 1), which is similar to the highest relative velocity observed between recording head and disk in high-end server HDDs. The recording head is then loaded against the moving counterface until the desired contact pressure is reached (step 2), calculated as the ratio of the normal load between the recording head and the rigid counterface and the cross-sectional area of the simulation box ( $x$ – $z$  plane). The moving counterface continuously slides against the head, resulting in combined normal and tangential loading (step 3). After sliding contact and

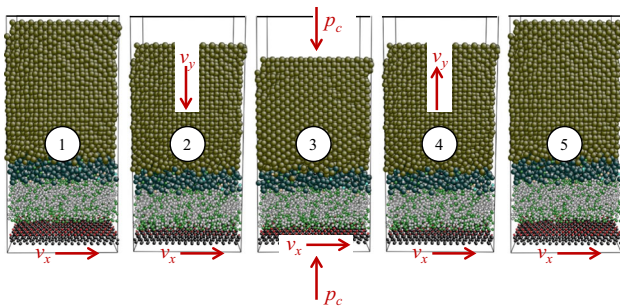


**Fig. 3** Schematic of combined normal and tangential loading procedure between the recording head and disk

combined loading, the head is separated from the moving counterface (step 4). The  $x$ -velocity of the disk is maintained constant until complete separation of head and counterface is obtained (step 5). We have performed simulations at a contact pressure  $p_c$  between the head and the counterface of 48 and 64 GPa, respectively.  $p_c$  is realistic for typical head/disk impact and is calculated based on measured wear areas and contact loads [8, 36]. They were also chosen to be slightly below the mean hardness of the coatings, which was measured to be 67.5 GPa in nanoindentation MD simulations, to give measurable deformation of the recording head in the short (130 ps) simulation time.

### 2.3 Deformation Analysis

We quantify deformation of the different coating layers and their interfaces by evaluating the number and length of the interatomic bonds of each bond type, throughout the simulation, relative to their respective equilibrium bond length. A bond exists between two atoms when their separation is less than a cutoff distance that falls between their first- and second-nearest neighbor distances [23]. The cutoff distance used for determining first-nearest neighbors and, thus, bonded versus non-bonded interactions is defined as the distance where the minimum between the first and second peaks of the radial distribution function (RDF) occurs for that bond type. Table 1 lists these cutoff values. The bond length is a function of the load and is quantified as strain. However, the bond cutoff is not affected by load and remains unchanged throughout the simulation. The equilibrium bond length is determined as the location of the first peak in the RDF. Figure 4 shows the RDF,  $g(r)$ , of the C–C bond type as an example. The location of the first peaks in the RDFs is within 1 % of the equilibrium reference structures for all atomic interactions except for Si–Si and C–C interactions. The location of the Si–Si peak results in an equilibrium bond length 8.7 % larger than predicted by the reference structure, because the amorphous Si layer conforms to the Ni face-centered cubic (FCC) lattice. The location of the C–C peak at 1.50 Å

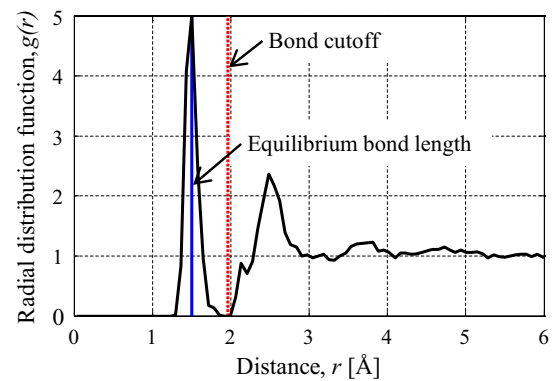


**Fig. 4** Radial distribution function for C–C interactions, for a recording head coating with  $t_{Si} = 3$  Å and  $t_C = 12$  Å. The values have been normalized with the maximum value at  $r = 6$  Å

**Table 1** Bond length and cohesive energy of each of the bond types in the MD model

Bond type	Equilibrium structure	Equilibrium bond length (Å)	RDF bond length (Å)	RDF bond cutoff (Å)	Cohesive energy [eV]
Ni–Ni	FCC	2.49 [27]	2.49	3.10	4.44 [38]
Ni–Si	112	2.41 [27]	2.40	2.77	5.51 [39]
Si–Si	Diamond	2.35 [33]	2.56	2.91	4.63 [40]
Si–C	3C–SiC	1.89 [33]	1.87	2.35	6.47 [41]
C–C	Diamond	1.54 [4]	1.50	1.96	7.84 [42]

The equilibrium bond length is also given for each bond type

The bond length and bond cutoff distance is determined from the radial distribution functions (RDF)

corresponds to the length of a bond between  $sp^3$ - and  $sp^2$ -hybridized carbon atoms [37], which is the prevailing structure in the amorphous mixture of  $sp^3$ - and  $sp^2$ -hybridized carbon atoms in the ta-C layer.

We define deformation on the atomic scale as a change in the number of bonds, with a permanent change in the number of bonds indicating plastic deformation and a permanent decrease in the number of bonds between two coating layers indicating delamination or separation in or between coating layers. Strain is calculated as the ratio of the change of the bond length between two atoms  $\Delta l$  and the equilibrium bond length between those atoms  $l_0$ . Local strain in the MD model is determined by overlaying a grid in the  $x$ – $y$  plane on the recording head and calculating the average strain of all the bonds with  $x$ - and  $y$ -coordinates that fall into each grid element, i.e.,  $\Sigma(\Delta l/l_0)/N_{\text{bonds}}$  for each grid element, where the summation is over the total number of bonds  $N_{\text{bonds}}$  in the grid element. Residual strain is quantified by calculating the strain in the coating before loading has occurred. It is a measure of the strain caused by

the difference in bond length and local structure mismatch near the Ni–Si and Si–C interfaces. Changes in the total bond energy throughout the head are also used to quantify deformation. Bond energy is calculated as the summation of the product of the number of bonds of a particular type  $N_T$  multiplied with the cohesive energy of that type  $E_T$  (see Table 1), i.e.,  $\Sigma(N_T * E_T)$ .

### 3 Results and Discussion

#### 3.1 Residual Strain

Figure 5 shows the mean residual strain in the recording head, prior to loading, as a function of  $t_{Si}$ , for different values of  $t_C$ . The mean residual strain decreases with increasing  $t_{Si}$ , but is almost independent of  $t_C$ . The mean bond length of Si–Si bonds, which is 8.7 % larger than the theoretical value (see Table 1), and the local strain visualizations (see Fig. 5) indicate that most of the strain is localized at the Ni–Si and Si–C interfaces. The Si layer conforms to the amorphous structure of the ta-C layer on one side and to the FCC lattice of Ni on the other side. As the thickness of the Si layer decreases, the transition from Ni to ta-C occurs over a smaller distance, increasing the local strain in the Si layer and surrounding interfaces due to the mismatch between the Ni, Si and ta-C structures.

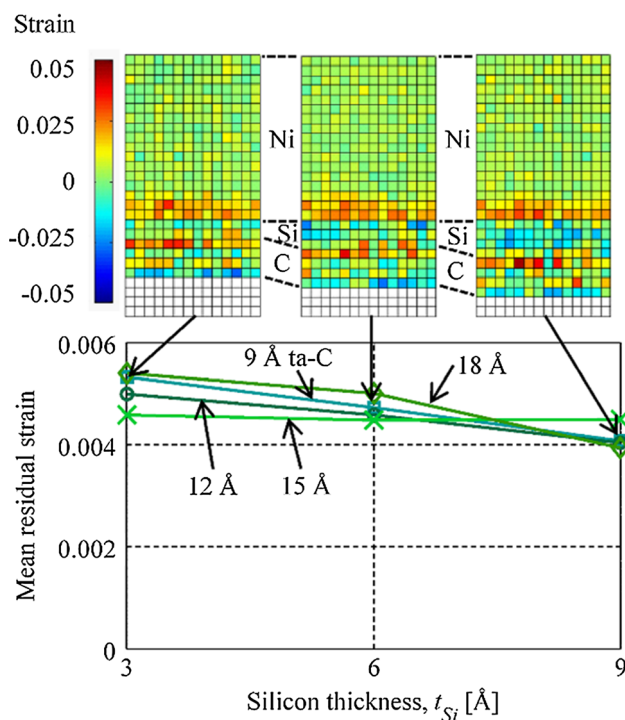


**Fig. 5** Mean residual strain in the recording head as a function of  $t_{Si}$  for different values of  $t_C$ . The corresponding plots of local residual strain are shown for the coatings with  $t_C = 9 \text{ \AA}$

#### 3.2 Deformation During Combined Loading

Figure 6 shows the instantaneous number of bonds for each bond type in the MD model, normalized with the initial number of bonds of that type, as a function of time during the combined loading simulation, for a DLC coating with  $t_{Si} = 3 \text{ \AA}$  and  $t_C = 12 \text{ \AA}$ , and for contact pressure  $p_c = 48 \text{ GPa}$  (Fig. 6a) and  $64 \text{ GPa}$  (Fig. 6b). The five steps shown in Fig. 3 are represented by three regions in Fig. 6. Region I corresponds to the initial equilibration and normal loading steps, region II corresponds to the combined normal and tangential loading, and region III corresponds to the unloading and separation steps. We observe that deformation occurs primarily in the Ni–Ni, Ni–Si, and Si–Si bonds during combined normal and tangential loading of the recording head and the rigid, moving counterface, because these bond types display the lowest cohesive energies of the different bond types in the recording head (see Table 1) and, thus, are easiest to deform. Although Ni–Ni bonds have the lowest cohesive energy, crystalline structures show higher intrinsic resistance to deformation compared to amorphous structures [43]. Hence, we observe deformation of the Ni–Si and Si–Si bonds before Ni–Ni bonds. As the load on the Ni substrate increases, the distance between second-nearest neighbor atoms is reduced

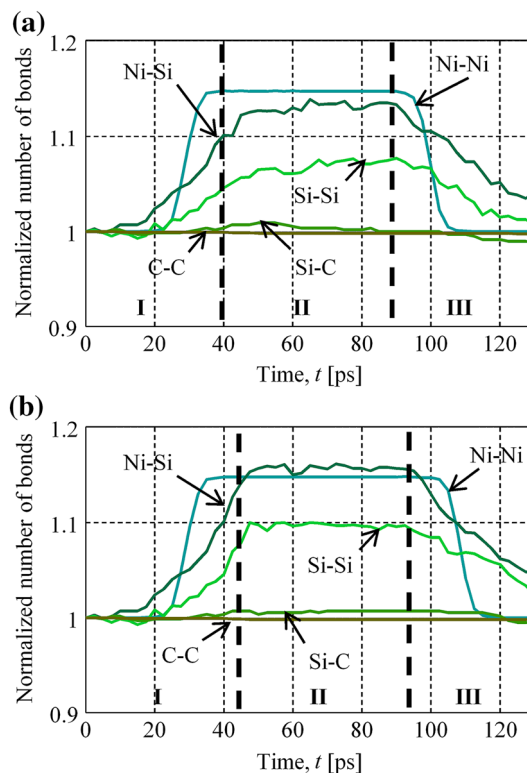
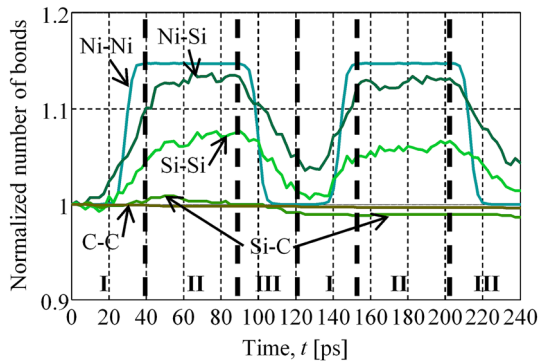


**Fig. 6** Instantaneous number of bonds of each bond type, normalized with the initial number of bonds of that type, versus time, for **a**  $p_c = 48 \text{ GPa}$  and **b**  $p_c = 64 \text{ GPa}$

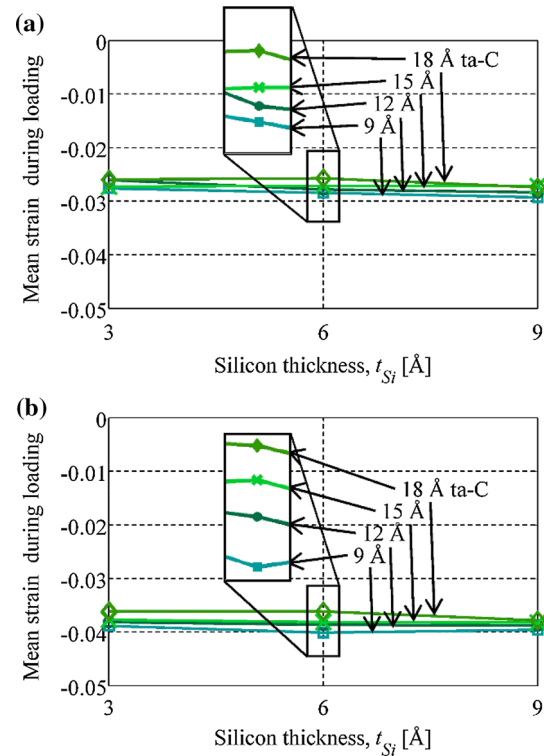
such that it falls within the first-nearest neighbor atom cutoff. This results in the steep increase in Ni–Ni bonds in region I (Fig. 6). The amorphous structure of the Ni–Si and Si–Si bond types results in a gradual deformation that increases with increasing contact pressure, illustrated in Fig. 6a and b. Limited deformation is observed in the Si–C interface and negligible deformation in the ta-C layer. However, the normalized number of Si–C bond is less than one after the combined loading procedure, indicating that this interface has been weakened by the loading. We do not observe wear or delamination of the DLC coating, which is likely due to the extremely short duration of the simulations.

Figure 7 shows the instantaneous number of bonds for each bond type in the MD model, normalized with the initial number of bonds of that type, as a function of time during two combined loading and unloading cycles for a DLC coating with  $t_{Si} = 3 \text{ \AA}$  and  $t_C = 12 \text{ \AA}$ , and for contact pressure  $p_c = 48 \text{ GPa}$ . Although the number of bonds during loading is similar in the first and second loading cycles for most bond types, we observe that the number of Si–C bonds decreases with repeated loading/unloading cycles, weakening the interface. The normalized number of Si–C bonds remains  $<1$  throughout the entire second combined loading/unloading procedure and results in a further loss of nearly 1 % of the Si–C bonds. Hence, this indicates that the Si–C damage is irreversible and will eventually lead to wear and delamination of the ta-C layer.

Figure 8 shows the mean strain in the recording head during combined loading, i.e., calculated during region II in Fig. 6, as a function of  $t_{Si}$  for different values of  $t_C$  and for  $p_c = 48 \text{ GPa}$  (Fig. 8a) and  $64 \text{ GPa}$  (Fig. 8b), respectively. The mean strain is negative due to compressive normal loading, and the magnitude increases with increasing contact pressure. The mean strain during loading becomes increasingly negative with increasing  $t_{Si}$ , similar to the results for the mean residual strain, which decreases



**Fig. 7** Instantaneous number of bonds of each bond type, normalized with the initial number of bonds of that type, versus time, for  $p_c = 48 \text{ GPa}$  during two cycles of combined loading and unloading



**Fig. 8** Mean strain in the recording head during combined loading as a function of  $t_{Si}$  for different values of  $t_C$  and for **a**  $p_c = 48 \text{ GPa}$  and **b**  $p_c = 64 \text{ GPa}$

with increasing  $t_{Si}$ . The higher residual tensile strain in the coatings with thinner  $t_{Si}$  counteracts the compressive loading, decreasing the deformation caused by compressive loading. Hence, coatings with higher residual tensile strain show less compressive strain during compressive loading. The magnitude of the mean strain during loading also decreases with increasing  $t_C$ , indicating that a thick carbon layer prevents deformation of the substrate. Due to the high cohesive energy of C–C bonds (see Table 1), it can absorb a large amount of energy compared to the rest of the coating without significantly deforming.

### 3.3 Permanent Deformation

Permanent deformation of each bond type in the recording head is quantified as the final number of bonds after combined loading relative to the initial number of bonds of that type. Figure 9a–c show the normalized final number of Ni–Si, Si–Si, and Si–C bonds, respectively, as a function of  $t_{Si}$ , for different values of  $t_C$  and for  $p_c = 64 \text{ GPa}$ . In each case, the final number of Ni–Si and Si–Si bonds increases by 0–6 % compared to the initial number of bonds, signifying strengthening of the Ni–Si interface. The final number of Si–C bonds changes by  $\pm 2 \%$  compared to the initial number of bonds, indicating that in certain cases, the Si–C interface is strengthened, and in other cases, it is

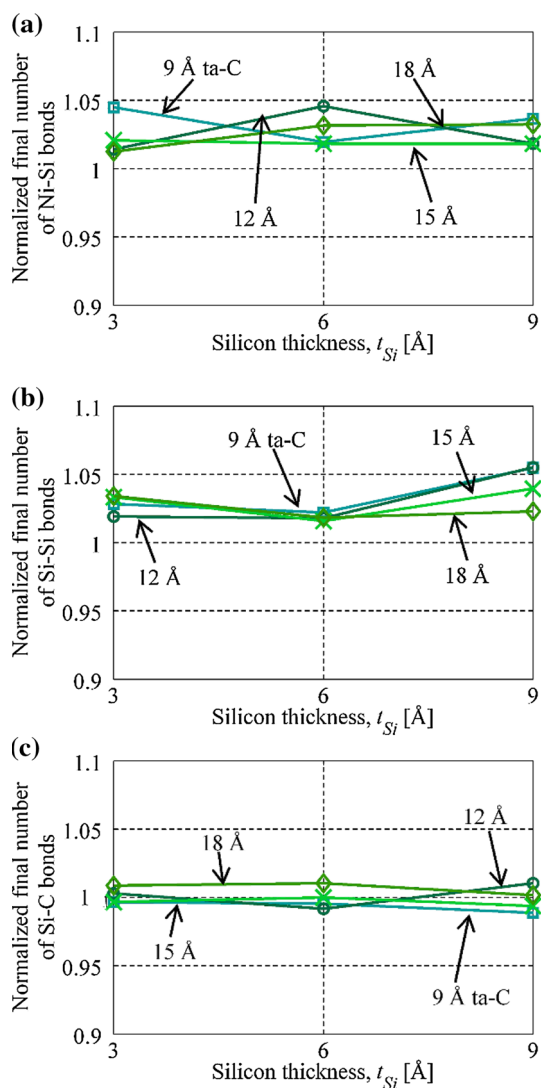


**Fig. 9** Final number of **a** Ni-Si bonds, **b** Si-Si bonds, and **c** Si-C bonds as a function of  $t_{Si}$  for different values of  $t_C$ , for the case of  $p_c = 64$  GPa. The final number of bonds has been normalized with the initial number of bonds

weakened by the combined external loading. During simulations with two combined loading cycles, such as the results shown in Fig. 7, we observe a decrease in the number of Si-C bonds after two loading cycles compared to one, indicating permanent deformation that accumulates each loading cycle and eventually will lead to wear and delamination between the Si and ta-C coating layers. The permanent deformation of the Ni-Si, Si-Si, and Si-C bonds seems nearly independent of  $t_C$  and  $t_{Si}$  for the cases investigated, especially in light of the stochastic nature of the MD simulations. The remaining bond types in the model, Ni-Ni and C-C, show negligible permanent deformation and are therefore not shown in Fig. 9. The C-C bonds have the highest cohesive energy compared to the other bond types, and, thus, no permanent deformation is

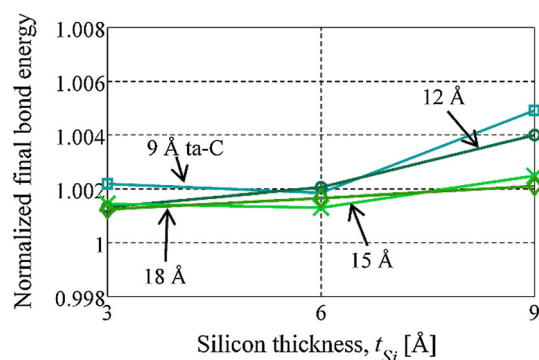


**Fig. 10** Final bond energy normalized with the initial bond energy as a function of  $t_{Si}$  for different values of  $t_C$

observed. The increase in the Ni-Ni bonds during loading, due to the temporary close proximity of second-nearest neighbor atoms, is purely elastic and fully recovered once the compressive loading is removed and the Ni atoms relax back into their equilibrium positions in the FCC lattice. It is the amorphous structure of the Ni-Si and Si-C interfaces as well as the Si layer in combination with the relatively low cohesive energies of those bond types that cause the only significant permanent deformation to occur in the Ni-Si and Si-Si bonds and to a lesser extent, Si-C bonds.

Figure 10 shows the normalized final bond energy as a function of  $t_{Si}$  for different values of  $t_C$  and for  $p_c = 64$  GPa, normalized with the initial bond energy. It is a measure of the total permanent deformation in the coating, i.e., the change in energy due to the deformation of the individual bond types shown in Fig. 9a-c. The final bond energy increases with increasing  $t_{Si}$  and decreasing  $t_C$ . The increase in final bond energy with increasing  $t_{Si}$  indicates that a thicker Si layer deforms more than a thinner Si layer at a given contact pressure. This deformation is due to the Si layer being the amorphous layer with the lowest cohesive energy. The increase in final bond energy with decreasing  $t_C$  agrees with the results shown in Fig. 8 and indicates that increasing  $t_C$  improves protection of the substrate due to the high C-C cohesive energy. The effect of  $t_C$  increases with increasing  $t_{Si}$ , which indicates that decreasing the ta-C layer has a bigger effect with increasing Si layer thickness. Thus, to optimize the strength of a DLC coating for a given coating thickness budget, it seems more effective to decrease  $t_{Si}$  before decreasing  $t_C$ .

#### 4 Conclusions

We have investigated the deformation of the DLC coating of a magnetic recording head during combined normal and tangential loading against a moving, rigid, hydrogen-terminated diamond counterface, simulating accidental contact. The

mean residual strain in the recording head decreases with increasing  $t_{Si}$ , but is independent of  $t_C$ , indicating that a thicker Si layer is desirable for reducing residual strain in the recording head. Deformation during combined loading and sliding occurs primarily in the Ni–Ni, Ni–Si, and Si–Si interactions and is a function of the cohesive energy and atomic structure of the layers. This deformation increases with decreasing  $t_C$ , indicating that a thicker carbon layer is desirable for protecting the recording head during combined loading and sliding contact. Permanent deformation is observed primarily in the Ni–Si and Si–C interfaces and in the Si layer and is also a function of the cohesive energy and atomic structure of the layers. Permanent separation between material layers is only observed in the Si–C interface and increases with additional combined loading cycles. The total permanent deformation of the DLC coating increases with increasing  $t_{Si}$  and decreasing  $t_C$ . Hence, to minimize deformation of the DLC coating under combined loading, for a given coating thickness budget, it is preferable to decrease the thickness of the Si layer before decreasing the thickness of the ta-C layer.

**Acknowledgments** The authors thank Western Digital Corporation for their support of this research, and Dr. Min Yang for her interest in this work. The support and resources from the Center for High Performance Computing at the University of Utah are gratefully acknowledged. We also acknowledge use of AtomEye [44].

## References

- Fontana, R., Hetzler, S., Decad, G.: Technology roadmap comparisons for tape, HDD, and NAND flash: implications for data storage applications. *IEEE Trans. Magn.* **48**, 1692–1696 (2012)
- Goglia, P., Berkowitz, J., Hoehn, J., Xidis, A., Stover, L.: Diamond-like carbon applications in high density hard disc recording heads. *Diam. Relat. Mater.* **10**, 271–277 (2001)
- Casiraghi, C., Robertson, J., Ferrari, A.: Diamond-like carbon for data and beer storage. *Mater. Today* **10**, 44–53 (2007)
- Robertson, J.: Diamond-like amorphous carbon. *Mater. Sci. Eng. R* **37**, 129–281 (2002)
- Wood, R.: Future hard drive systems. *J. Magn. Magn. Mater.* **321**, 555–561 (2009)
- Sander, P., Kaiser, U., Altebockwinkel, M., Wiedmann, L., Benninghoven, A., Sah, R., Koidl, P.: Depth profile analysis of hydrogenated carbon layers on silicon by X-ray photoelectron spectroscopy, Auger electron spectroscopy, electron energy-loss spectroscopy, and secondary ion mass spectrometry. *J. Vac. Sci. Technol. A* **5**(4), 1470–1473 (1987)
- Peng, W., Kiely, J., Hsia, Y.: Wear analysis of head-disk interface during contact. *J. Tribol. T ASME* **127**, 171–179 (2005)
- Song, D., Kvitik, R., Schnur, D.: Inspection of pole tip diamondlike carbon wear due to heater-induced head–disc contact. *J. Appl. Phys.* **99**, 08N107 (2006)
- Erdemir, A., Donnet, C.: Tribology of diamond-like carbon films: recent progress and future prospects. *J. Phys. D Appl. Phys.* **39**, R311–R327 (2006)
- Hauert, R.: An overview on the tribological behavior of diamond-like carbon in technical and medical applications. *Tribol. Int.* **37**, 991–1003 (2004)
- Liu, Y., Erdemir, A., Meletis, E.: An investigation of the relationship between graphitization and frictional behavior of DLC coatings. *Surf. Coat. Technol.* **86–87**, 564–568 (1996)
- Yamamoto, T., Hyodo, H.: Amorphous carbon overcoat for thin-film disk. *Tribol. Int.* **36**, 483–487 (2003)
- Ferrari, A.: Diamond-like carbon for magnetic storage disks. *Surf. Coat. Technol.* **180**, 190–206 (2004)
- Robertson, J.: Ultrathin carbon coatings for magnetic storage technology. *Thin Solid Films* **383**, 81–88 (2001)
- Prabhakaran, V., Talke, F.: Wear and hardness of carbon overcoats on magnetic recording sliders. *Wear* **243**, 18–24 (2000)
- Lee, K., Yeo, C., Polycarpou, A.: Nanomechanical property and nanowear measurements for sub-10-nm thick films in magnetic storage. *Exp. Mech.* **47**, 107–121 (2007)
- Zhong, M., Zhang, C., Luo, J., Lu, X.: The protective properties of ultra-thin diamond like carbon films for high density magnetic storage devices. *Appl. Surf. Sci.* **256**, 322–328 (2009)
- Yasui, N., Inaba, H., Furusawa, K., Saito, M., Ohtake, N.: Characterization of head overcoat for 1 Tb/in<sup>2</sup> magnetic recording. *IEEE Trans. Magn.* **45**(2), 805–809 (2009)
- Gao, G., Cannara, R., Carpick, R., Harrison, J.: Atomic-scale friction on diamond: a comparison of different sliding directions on (001) and (111) surfaces using MD and AFM. *Langmuir* **23**, 5394–5405 (2007)
- Wang, C., Ho, K.: Structure, dynamics, and electronic properties of diamondlike amorphous carbon. *Phys. Rev. Lett.* **71**(8), 1184–1187 (1993)
- Ma, T., Hu, T., Wang, H., Li, X.: Microstructural and stress properties of ultrathin diamondlike carbon films during growth: molecular dynamics simulations. *Phys. Rev. B* **75**, 035425 (2007)
- Ma, T., Hu, Y., Wang, H.: Molecular dynamics simulation of shear-induced graphitization of amorphous carbon films. *Carbon* **4**(7), 1953–1957 (2009)
- Gao, G., Mikulski, P., Harrison, J.: Molecular-scale tribology of amorphous carbon coatings: effects of film thickness, adhesion, and long-range interactions. *J. Am. Chem. Soc.* **124**(24), 7202–7209 (2002)
- Wang, N., Komvopoulos, K.: Nanomechanical and friction properties of ultrathin amorphous carbon films studied by molecular dynamics analysis. *ASME Conf. Proc.* **2010**(44199), 393–395 (2010)
- Glosli, J., Belak, J., Philpott, M.: Ultra-thin carbon coatings for head–disk interface tribology. *Mater. Res. Soc. Symp. Proc.* **356**, 749–753 (1995)
- Iwasaki, T., Miura, H.: Analysis of adhesion strength of interfaces between thin films using molecular dynamics technique. *Mater. Res. Soc. Symp. Proc.* **594**, 377–382 (1999)
- Baskes, M., Angelo, J., Bisson, C.: Atomistic calculations of composite interfaces. *Model. Simul. Mater. Sci.* **2**(3A), 505–518 (1999)
- Deng, H., Minor, K., Barnard, K.: Comparison of mechanical and tribological properties of permalloy and high moment FeTaN thin films for tape recording heads. *IEEE Trans. Magn.* **32**, 3702–3704 (1996)
- Ma, Z., Long, S., Pan, Y., Zhou, Y.: Creep behavior and its influence on the mechanics of electrodeposited nickel films. *J. Mater. Sci. Technol.* **25**, 90–94 (2009)
- Frick, C., Clarck, B., Orso, S., Schneider, A., Arzt, E.: Size effect and strain hardening of small-scale [111] nickel compression pillars. *Mater. Sci. Eng. A* **489**, 319–329 (2008)
- Klokholm, E., Aboaf, J.: The saturation magnetostriction of permalloy films. *J. Appl. Phys.* **52**, 2474–2476 (1981)
- Baskes, M.: Modified embedded-atom potentials for cubic materials and impurities. *Phys. Rev. B* **46**, 2727–2742 (1992)
- Tersoff, J.: New empirical approach for the structure and energy of covalent systems. *Phys. Rev. B* **37**, 6991–7000 (1988)

34. Stuart, S., Tutein, A., Harrison, J.: A reactive potential for hydrocarbons with intermolecular interactions. *J. Chem. Phys.* **112**, 6472–6486 (2000)
35. Plimpton, S.: Fast parallel algorithms for short-range molecular dynamics. *J. Comput. Phys.* **117**(1), 1–19 (1995)
36. Mate, C., Arnett, P., Baumgart, P., Dai, Q., Guruz, U., Knigge, B., Payne, R., Ruiz, O., Wang, G., Yen, B.: Dynamics of contacting head–disk interfaces. *IEEE Trans. Magn.* **40**, 3156–3158 (2004)
37. Lide Jr, D.: A survey of carbon–carbon bond lengths. *Tetrahedron* **17**, 125–134 (1962)
38. Bylander, D., Kleinman, L., Mednick, K.: Self-consistent energy bands and bonding of  $\text{Ni}_3\text{Si}$ . *Phys. Rev. B* **25**, 1090–1095 (1982)
39. Bylander, D., Kleinman, L., Mednick, K., Grise, W.: Self-consistent energy bands and bonding of  $\text{NiSi}_2$ . *Phys. Rev. B* **26**, 6379–6383 (1982)
40. Zirklebach, F.: Atomistic simulation study on silicon carbide precipitation in silicon. PhD thesis, University of Augsburg (2011)
41. Bekaroglu, E., Topsakal, M., Cahangirov, S., Ciraci, S.: A first-principles study of defects and adatoms in silicon carbide honeycomb structures. *Phys. Rev. B* **81**, 075433 (2010)
42. Chelikowsky, J.: First principles linear combination of atomic orbitals method for the cohesive and structural properties of solids: application to diamond. *Phys. Rev. B* **29**, 3470–3481 (1984)
43. Szlufarska, I., Kalia, R., Nakano, A., Vashishta, A.: A molecular dynamics study of nanoindentation of amorphous silicon carbide. *J. Appl. Phys.* **102**, 023509 (2007)
44. Li, J.: AtomEye: an efficient atomistic configuration viewer. *Model. Simul. Mater. Sci.* **11**(2), 173–177 (2003)